Chemical Geology 391 (2015) 7–18

Contents lists available at ScienceDirect

Chemical Geology

journal homepage: www.elsevier.com/locate/chemgeo

The influence of pH on barite nucleation and growth

Cristina Ruiz-Agudo [a,*], Christine V. Putnis [a], Encarnación Ruiz-Agudo [b], Andrew Putnis [a]

[a] Institut für Mineralogie, University of Münster, Corrensstrasse 24, 48149 Münster, Germany
[b] Departament of Mineralogy and Petrology, University of Granada, Fuentenueva s/n, 18071 Granada, Spain

ARTICLE INFO

Article history:
Received 29 May 2014
Received in revised form 20 October 2014
Accepted 23 October 2014
Available online 4 November 2014

Editor: J. Fein

Keywords:
Barite growth
Atomic Force Microscopy
AFM
pH dependence

ABSTRACT

Nanoscale Atomic Force Microscopy (AFM) experiments show that barite ($BaSO_4$) growth is influenced by the pH of the growth solution. AFM observations provide evidence that growth and nucleation rates measured along the [100] crystallographic direction on the initial layer grown on barite (001) natural surfaces increase at both high and low pH of the growth solutions. At alkaline pH, growth is arrested in the second and successive layers, possibly as a result of the structure distortion resulting from incorporation of foreign ions (OH^- and/or CO_3^{2-}). Macroscopic nucleation experiments also show that with increasing pH, the induction times, the precipitation rate and the interfacial tension are all reduced, consistent with nanoscale observations. Smaller particle size at high pH provides further evidence for enhanced barium sulfate nucleation in alkali solutions. This enhancement in growth as well as in nucleation of barite at high pH could be explained by taking into account the effect of hydroxyl ions on hydration shells of aqueous Ba^{2+} and SO_4^{2-} in solution and on the barite surface. The energetic interaction between water molecules and the barite building units is affected by the presence of OH^- ions in solution. The frequency of water exchange around Ba^{2+} and SO_4^{2-} could increase due to the effect of OH^- ions on the structure of water and consequently promote nucleation and growth. Increased growth at low pH can be attributed to increased Ba^{2+} activity with respect to SO_4^{2-}.

1. Introduction

Barite scale formation is a major problem in many industrial processes, including paper-making, chemical manufacturing, cement operations, off-shore oil extraction, and geothermal energy production (Todd and Yuan, 1990). It is especially problematic (and costly) in oilfields due to its low solubility, resulting in solid layers of barite scale that can block pipes and reservoir rocks, reducing the production of an oil well. Barite scale in oilfields results from mixing the injected seawater containing SO_4^{-2} (to maintain pressure within the reservoir and therefore increase the oil extraction) and formation of water (containing Ba^{2+}) in the reservoir.

The incorporation of trace amounts of radium (Ra^{2+}) into barite, due to the similarity to Ba^{2+} in ionic radius and charge (Hanor, 2000) also leads to the problem that the scale can be radioactive (Ceccarello et al., 2003). Depending on the location of the precipitates, the techniques used to remove barite scales can be "mechanical" or "chemical" treatments, the latter based on the use of chemical compounds — such as chelating agents (commonly used diethylenetriamine pentaacetic acid, DTPA or ethylenediamine triacetic acid, EDTA) or various inhibitors such as organophosphonates (sodium phosphonobutane tricarboxylic acid, PBTC; nitro trimethyl phosphonic acid, NTMP; methylene diphosphonic acid, MDP; hydroxyethylene diphosphonic acid, HEDP; amino methylene phosphonic acid, AMP). The effectiveness of these compounds is pH-dependent, usually more effective at high pH where they are highly deprotonated (Van Rosmalen, 1983). Jones et al. (2002) studied the effect of various phosphonate inhibitors on barium sulfate precipitation and they found that the best inhibition effect of these inhibitors tested was at pH 8. Because barium sulfate is highly insoluble ($\log K_{sp\ (25\ °C)} = -9.96$, Blount, 1977), both chemical approaches for scale prevention involving chelation (dissolution) or inhibition (control of crystal growth) have limited success and sometimes it is finally necessary to shut down the oil production and replace the damaged pipes with the subsequent economic consequences.

In the case of chemical treatments, unsuccessful results are also related to the fact that the mechanisms of $BaSO_4$ scale formation and those by which the "chemical" methods could reduce or prevent it are in general poorly understood. To be able to control crystal growth, we first need to know how barite grows, the conditions for optimal growth, as well as any factors that inhibit or reduce its nucleation and growth to a minimum. This is a crucial first step for the development of more effective tools for scale prevention or removal treatments. Due to the dependence of the effectiveness of barite scale inhibitors on pH, we consider that it is important to determine the influence of pH on barite nucleation and growth before the performance of organic additives as barite scale inhibitors can be fully assessed. To the best of our knowledge there has been no previous published research on the pH dependence on the growth of barite. Dove and Czank (1995) studied

* Corresponding author.

http://dx.doi.org/10.1016/j.chemgeo.2014.10.023
0009-2541/

the pH effect on the dissolution of barite but no other published studies have been carried out on the influence of pH on barite growth or dissolution.

To unambiguously assess the role of solution pH on barite growth, other solution parameters influencing the kinetics or mechanisms of $BaSO_4$ formation need to be held constant. The three main solution parameters which may affect barite growth kinetics and mechanisms are: saturation index (SI) expressed as $SI = \log (IAP/K_{sp})$ where IAP is ion activity product and K_{sp} is the solubility product; ionic strength (IS) and Ba^{2+} and SO_4^{-2} activities. All of these parameters are interrelated, so that changing the pH of the growth solution alters IS, speciation, Ba^{2+} and SO_4^{-2} activities and consequently SI. Thus varying the pH of the experimental solution also introduces changes in the other parameters.

The main goal of this study is to gain a better understanding of the effect of pH on barite two-dimensional (2D) nucleation and growth and to corroborate or compare these nanoscale findings with 3D-nucleation observations. This has been done by carrying out in situ AFM observations during the growth of (001) barite surfaces, turbidity and conductivity precipitation experiments as well as calorimetric measurements on barite crystallization.

2. Experimental procedure

2.1. AFM experiments

AFM experiments were performed at room temperature (22 °C ± 2 °C) in a fluid cell of a Digital Instruments (Bruker) Multimode AFM, Nanoscope IIIa working in contact mode. Optically clear barite single crystals from Arran (Scotland) were used for the experiments. Electron microprobe analysis of a polished section of the crystals showed no measurable chemical zonation and a composition of 99.7–99.5 mol% $BaSO_4$, with minor $SrSO_4$ and $CaSO_4$ (up to 0.3–0.5 mol%) in solid solution. The crystals were cleaved immediately before each experiment to obtain a fresh (001) surface. Growth solutions were injected into the fluid cell before each AFM scan, giving a flow rate of approximately 80 ml/h. Previous results suggest that, under such flow conditions, growth is surface controlled (e.g. Kowacz and Putnis, 2008) rather than diffusion controlled. Images and time were continuously recorded so that it was possible to measure growth rates in different crystallographic directions, using the Nanoscope software (Bruker).

$BaSO_4$ growth solutions were prepared immediately prior to each experiment from stock solutions made from solids from Merck Suprapur min. 99.995% ($BaCl_2$) and Aldrich min. 99% (Na_2SO_4) and deionized water (Milli-Q, resistivity >18.2 MΩ·cm). The pH and ionic strength (IS) were adjusted by the addition of NaOH or HCl and NaCl aqueous solutions, respectively. No attempt was made to remove CO_2 from the growth solutions since PHREEQC simulations (Parkhurst and Appelo, 1999) indicated that its presence does not significantly influence the saturation state of the solution with respect to barium sulfate.

Therefore, once NaOH or HCl was added to adjust the pH of the growth solutions, with the consequent increase in ionic strength and the decrease of the mean activity coefficients of aqueous Ba^{2+} and SO_4^{-2}, Ba^{2+} and SO_4^{-2} concentrations had to be slightly increased in order to keep the SI approximately constant during our experiments. The saturation index with respect to barite (SI) varies in all growth experiments between 0.92 and 0.94. The speciation software PHREEQC (Parkhurst and Appelo, 1999) was used to calculate SI, IS and pH. The pH of the solutions was also confirmed with a pH meter. Potential equilibration of the solutions with atmospheric CO_2 was taken into account in all the PHREEQC simulations. For dilute electrolyte solutions (IS < 0.1), the activity coefficients are described by the Debye–Hückel equation as a function of IS and the increase in the IS results in a decrease in the activity coefficients. This directly influences the IAP and consequently the SI of the solution. Another consequence of the variation in the solution pH is the change in concentration of different species present in solution that includes the concentration of building units (Ba^{2+} and SO_4^{2-}) and therefore the IAP and consequently the SI. For our specific case, the speciation does not vary significantly when working at high pH solutions but in acidic solutions the [HSO_4^-] species increased so that at pH 2 the concentration of $BaSO_4$ had to be significantly adjusted in order to maintain the same SI as in all other experiments.

To check whether differences in IS of growth solutions when pH was being changed were responsible for the observed change in growth rates, we performed three additional growth experiments at neutral pH in which NaCl was added to obtain the same IS as that of the growth solutions of pH 2, pH 10 and pH 11 (Table 1). The SI was kept constant (0.94) and in order to achieve this, the concentration of Ba^{2+} and SO_4^{-2} had to be slightly adjusted.

All the images were analyzed using the software NanoScope 1.40 Analysis and the computer design program AUTOCAD 2013. Growth rates along the [100] direction on sector-shaped growth islands are reported as the average value determined for each experiment taken from at least 3–5 growth islands per scan. Errors in the measured rates were calculated as the standard deviation (σ) and the experiments were repeated at least twice to ensure that errors were below 15%. A rough quantification of nucleation density was performed by counting the number of nuclei in a given area of 5 × 5 μm after 270 s injecting solution (Baynton et al., 2012). The induction time was determined as the time at which the first nuclei were observed on the surface. The composition of the different solutions used in AFM experiments is shown Table 1.

2.2. Nucleation experiments

The induction time for nucleation (t_{ind}) was defined as the elapsed time between the moment at which supersaturation is reached (by mixing of $BaCl_2$ and Na_2SO_4 solutions) and that at which a critical nucleus is observed (Söhnel and Mullin, 1978). Our approach to measure t_{ind} was to observe changes in various physical properties of the mixed solution, as outlined below.

2.2.1. Turbidity experiments

In a first set of experiments, nucleation was determined by monitoring the variation in solution turbidity (measured as absorbance) using UV–visible spectrophotometry. These experiments were carried out at room temperature by mixing equal volumes (1 ml) of $BaCl_2$ and Na_2SO_4 solutions with different pH values (2, 6.5, 8.5, 10, 11, 12) in a fluid cell, resulting in a solution supersaturated with respect to barium sulfate. The range of concentrations used in these experiments varied from 1.5×10^{-4} M to 4×10^{-4} M. The evolution of the absorbance of the mixed solutions was monitored at 600 nm using a Cary 50 UV–Vis spectrophotometer. Changes in the absorbance of the solution due to the precipitation of barite were used to determine the induction time. The induction time was determined by the intersection between the line tangent to the absorbance plot in the initial stages of the experiment and the line corresponding to the linear increase in the absorbance stage. Measurements were repeated at least 4 times to ensure reproducibility of the results. After the experiments, the barite precipitates formed in 1.5×10^{-4} M solutions with different pH values were filtered (0.45 μm pore diameter), washed and then dried for 24 h at 40 °C before analysis by field emission scanning electron microscopy (Auriga Carl Zeiss SMT). This FESEM was equipped with Energy Dispersive X-ray analysis (EDX) that allows us to characterize the particles obtained.

The interfacial tension between a crystalline solid and a solution of the dissolved solid is an important parameter to characterize crystal growth and nucleation processes (Nielsen and Söhnel, 1971). According to the classical nucleation theory (Mullin, 1992) we can express the rate

Table 1
Composition and speciation of solutions used in AFM experiments. IS denotes ionic strength. Values calculated with Parkhurst and Appelo (1999).

	SI_{Barite}	$[BaSO_4]$ (μM)	IS	pH	[NaCl] (M)	[NaOH] (M)	[HCl] (M)	$a(Ba^{2+})$	$a(BaOH^+)$	$a(BaSO_4^0)$	$a(BaCO_3^0)$	$a(BaHCO_3^+)$	$a(SO_4^{-2})$	$a(NaSO_4^-)$	$a(HSO4^-)$
BARITE 1	0.93	54	$1.129 * 10^{-2}$	2	0	0	$1.101 * 10^{-2}$	$3.487 * 10^{-5}$	$1.181 * 10^{-16}$	$3.749 * 10^{-7}$	$5.027 * 10^{-20}$	$2.092 * 10^{-13}$	$2.145 * 10^{-5}$	$1.011 * 10^{-8}$	$1.874 * 10^{-5}$
BARITE 2	0.94	34	$1.238 * 10^{-3}$	3	0	0	$1.040 * 10^{-3}$	$2.875 * 10^{-5}$	$9.743 * 10^{-16}$	$3.848 * 10^{-7}$	$4.133 * 10^{-18}$	$1.720 * 10^{-12}$	$2.670 * 10^{-5}$	$8.474 * 10^{-9}$	$2.333 * 10^{-6}$
BARITE 3	0.93	30	$2.801 * 10^{-4}$	4	0	0	$1.020 * 10^{-4}$	$2.745 * 10^{-5}$	$9.302 * 10^{-15}$	$3.746 * 10^{-7}$	$3.926 * 10^{-16}$	$1.635 * 10^{-11}$	$2.723 * 10^{-5}$	$7.778 * 10^{-9}$	$2.379 * 10^{-7}$
BARITE 4	0.94	30	$1.885 * 10^{-4}$	5	0	0	$9.435 * 10^{-6}$	$2.781 * 10^{-5}$	$9.424 * 10^{-14}$	$3.873 * 10^{-7}$	$3.836 * 10^{-14}$	$1.596 * 10^{-10}$	$2.779 * 10^{-5}$	$7.964 * 10^{-9}$	$2.428 * 10^{-8}$
BARITE 5	0.94	30	$1.810 * 10^{-4}$	6–7	0	0	0	$2.784 * 10^{-5}$	$3.750 * 10^{-13}$	$3.885 * 10^{-7}$	$5.415 * 10^{-13}$	$5.670 * 10^{-10}$	$2.784 * 10^{-5}$	$7.981 * 10^{-9}$	$6.119 * 10^{-9}$
BARITE 6	0.94	30	$2.044 * 10^{-4}$	9	0	$2.530 * 10^{-5}$	0	$2.773 * 10^{-5}$	$9.396 * 10^{-10}$	$3.855 * 10^{-7}$	$9.019 * 10^{-9}$	$3.754 * 10^{-9}$	$2.774 * 10^{-5}$	$1.129 * 10^{-8}$	$2.424 * 10^{-12}$
BARITE 7	0.93	30	$2.765 * 10^{-4}$	10	0	$9.228 * 10^{-5}$	0	$2.739 * 10^{-5}$	$9.282 * 10^{-9}$	$3.769 * 10^{-7}$	$6.409 * 10^{-8}$	$2.667 * 10^{-9}$	$2.745 * 10^{-5}$	$1.998 * 10^{-8}$	$2.399 * 10^{-13}$
BARITE 8	0.93	32	$9.446 * 10^{-4}$	11	0	$7.409 * 10^{-4}$	0	$2.734 * 10^{-5}$	$9.265 * 10^{-8}$	$3.768 * 10^{-7}$	$1.588 * 10^{-7}$	$6.610 * 10^{-10}$	$2.750 * 10^{-5}$	$1.038 * 10^{-7}$	$2.403 * 10^{-14}$
BARITE 9	0.91	40	$7.799 * 10^{-3}$	12	0	$7.550 * 10^{-3}$	0	$2.671 * 10^{-5}$	$9.048 * 10^{-7}$	$3.609 * 10^{-7}$	$1.394 * 10^{-7}$	$5.802 * 10^{-11}$	$2.696 * 10^{-5}$	$9.115 * 10^{-7}$	$2.355 * 10^{-15}$
BARITE 10[a]	0.93	30	$3.100 * 10^{-4}$	6–7	$1.290 * 10^{-4}$	0	0	$2.735 * 10^{-5}$	$3.682 * 10^{-13}$	$3.745 * 10^{-7}$	$5.316 * 10^{-13}$	$5.568 * 10^{-10}$	$2.733 * 10^{-5}$	$2.456 * 10^{-8}$	$6.008 * 10^{-8}$
BARITE 11[b]	0.94	32	$8.911 * 10^{-4}$	6–7	$7.023 * 10^{-4}$	0	0	$2.767 * 10^{-5}$	$3.724 * 10^{-13}$	$3.826 * 10^{-7}$	$5.374 * 10^{-13}$	$5.630 * 10^{-10}$	$2.759 * 10^{-5}$	$9.873 * 10^{-8}$	$6.070 * 10^{-8}$
BARITE 12[c]	0.93	43	$1.131 * 10^{-2}$	6–7	$1.106 * 10^{-2}$	0	0	$2.770 * 10^{-5}$	$3.704 * 10^{-13}$	$3.744 * 10^{-7}$	$5.310 * 10^{-13}$	$5.600 * 10^{-10}$	$2.697 * 10^{-5}$	$1.311 * 10^{-6}$	$5.970 * 10^{-9}$
BARITE 13	0.93	32	$9.446 * 10^{-4}$	11	0	$7.409 * 10^{-4}$	0	$2.734 * 10^{-5}$	$9.265 * 10^{-8}$	$3.768 * 10^{-7}$	$1.588 * 10^{-7}$	$6.610 * 10^{-10}$	$2.750 * 10^{-5}$	$1.038 * 10^{-7}$	$2.403 * 10^{-14}$
(Recovery)	1.35	53	$1.069 * 10^{-3}$	11	0	$7.425 * 10^{-4}$	0	$4.459 * 10^{-5}$	$1.511 * 10^{-7}$	$1.002 * 10^{-6}$	$2.558 * 10^{-6}$	$1.065 * 10^{-9}$	$4.484 * 10^{-5}$	$1.780 * 10^{-7}$	$3.917 * 10^{-14}$

[a] IS_{pH10}, IS same as pH 10 growth solution.
[b] IS_{pH11}, IS same as pH 11 growth solution.
[c] IS_{pH2}, IS same as pH 2 growth solution.

of nucleation (J) (number of nuclei formed per unit time per unit volume) in the form of Arrhenius reaction velocity equation:

$$J = A * e\left(\frac{-\Delta G^*}{kT}\right)$$

where A is a constant, ΔG^* is the free activation energy for the formation of a critical nucleus, k is the Boltzmann's constant ($1.3805 * 10^{-23}$ J/K) and T is the absolute temperature (K).

ΔG^* can be expressed as:

$$\Delta G^* = \frac{\beta * \gamma^3 * \nu^2}{(k * T * \ln(S))^2}$$

where β is a dimensionless factor that depends on the shape of the nucleus ($16\pi/3$ for spherical nucleus), γ is the interfacial tension, ν is molecular volume ($8{,}65 * 10^{-29}$ m^3/molecule) and S is the supersaturation ($a(Ba^{2+}) * a(SO_4^{-2}) / K_{sp}$).

It is clear that the induction time (t_{ind}) is inversely proportional to the nucleation rate (J) and can be expressed as:

$$\ln(t_{ind}) \sim A + \frac{\beta * \gamma^3 * \nu^2}{(k * T * \ln(S))^2}.$$

Therefore, by plotting the $\ln(t_{ind})$ versus $\ln(S)^{-2}$ we should find a linear dependence that allows estimation of the crystal-solution interfacial tension (γ) from the slope of the line. This parameter (γ) obtained from nucleation and crystallization of a solvent-solute system can be difficult to interpret as a true physical value (interfacial tension), however, its use as an approach to quantify crystallization processes is justified by Söhnel (1982). Values of γ from kinetics of nucleation of partially miscible liquids were found to be in agreement with macroscopic values obtained experimentally.

2.2.2. Conductivity experiments

Conductivity experiments were carried out with the aim of determining the rate of change in conductivity during barium sulfate precipitation. Plots of conductivity versus time were used to obtain an estimation of the precipitation rate from the slope of the linear region of the curve (Jones et al., 2002). These precipitation experiments were carried out at controlled temperature (20 °C) in a jacketed reaction vessel, under continuous magnetic stirring to keep the solids in suspension. Supersaturation was achieved by mixing 100 ml of $BaCl_2$ solution with 100 ml Na_2SO_4 (both solutions with the corresponding tested pH). Upon mixing of the solutions, the pH and conductivity of the solution using a pH and conductivity-meter (905 Titrando, Methrom) were continuously monitored. The natural pH was measured and found to be 5.5–6. NaOH and HCl were used to adjust the pH of $BaCl_2$ and Na_2SO_4 solutions. The Saturation Index (SI) was kept constant in all the experiments with a value 2.16.

After the conductivity experiments, the solutions were filtered through cellulose nitrate membrane filters (Millipore®, pore size 0.45 μm) and barite particles were dried at 40 ° C for 24 h before carbon coating and subsequent analysis by field emission scanning electron microscopy (Auriga Carl Zeiss SMT). This FESEM is equipped with Energy Dispersive X-ray analysis (EDX), allowing compositional characterization of the particles obtained.

2.3. Calorimetric experiments

A calorimeter (PARR 6755) equipped with a PARR 6772 high-precision thermometer was used to measure the heat of precipitation of barium sulfate from solutions at different pH values. $BaSO_4$ precipitation occurred upon mixing $BaCl_2$ and Na_2SO_4 solutions that were prepared using doubly-deionized (MilliQ) water (resistivity

>18.2 MΩ·cm). The Dewar flask in the calorimeter was filled with 100 ml of a $1.65 \cdot 10^{-3}$ M Na_2SO_4 solution and 10 ml of $1.65 \cdot 10^{-2}$ M $BaCl_2$ solution were loaded into a glass cell sealed with a detachable Teflon dish. The glass cell was introduced in the Dewar flask and rotated by an external electric motor. As soon as the thermal equilibrium was reached, the $BaCl_2$ solution in the cell was poured out and the reactants were mixed. The electric motor then stopped and the calorimeter measured the change in temperature once the precipitation process had taken place. The solution was filtered through a 0.45 μm pore diameter filter after each experiment and then analyzed by ICP-AES (inductively coupled plasma atomic emission spectroscopy) to obtain the final Ba^{2+} concentration. The difference in the Ba^{2+} concentration before and after the precipitation process is assumed to be due to the stoichiometric formation of $BaSO_4$, and thus the number of moles of barite precipitate could be calculated.

The heat released during barium sulfate precipitation (Q_{BaSO_4}) was estimated by multiplying the measured temperature change (ΔT_c) and the energy equivalent (e) of the calorimeter and its contents: $Q_{BaSO4} = \Delta T_c * e$ (e was determined by a pre-experimental standardization process). Once Q_{BaSO_4} was obtained, the enthalpy of precipitation ΔH_{ppt} was calculated as: $-Q_{BaSO_4} / N$, where N was the number of moles precipitated. These calorimetric measurements were not aimed at determining accurate absolute values for the enthalpy of barium sulfate precipitation, but to allow comparison

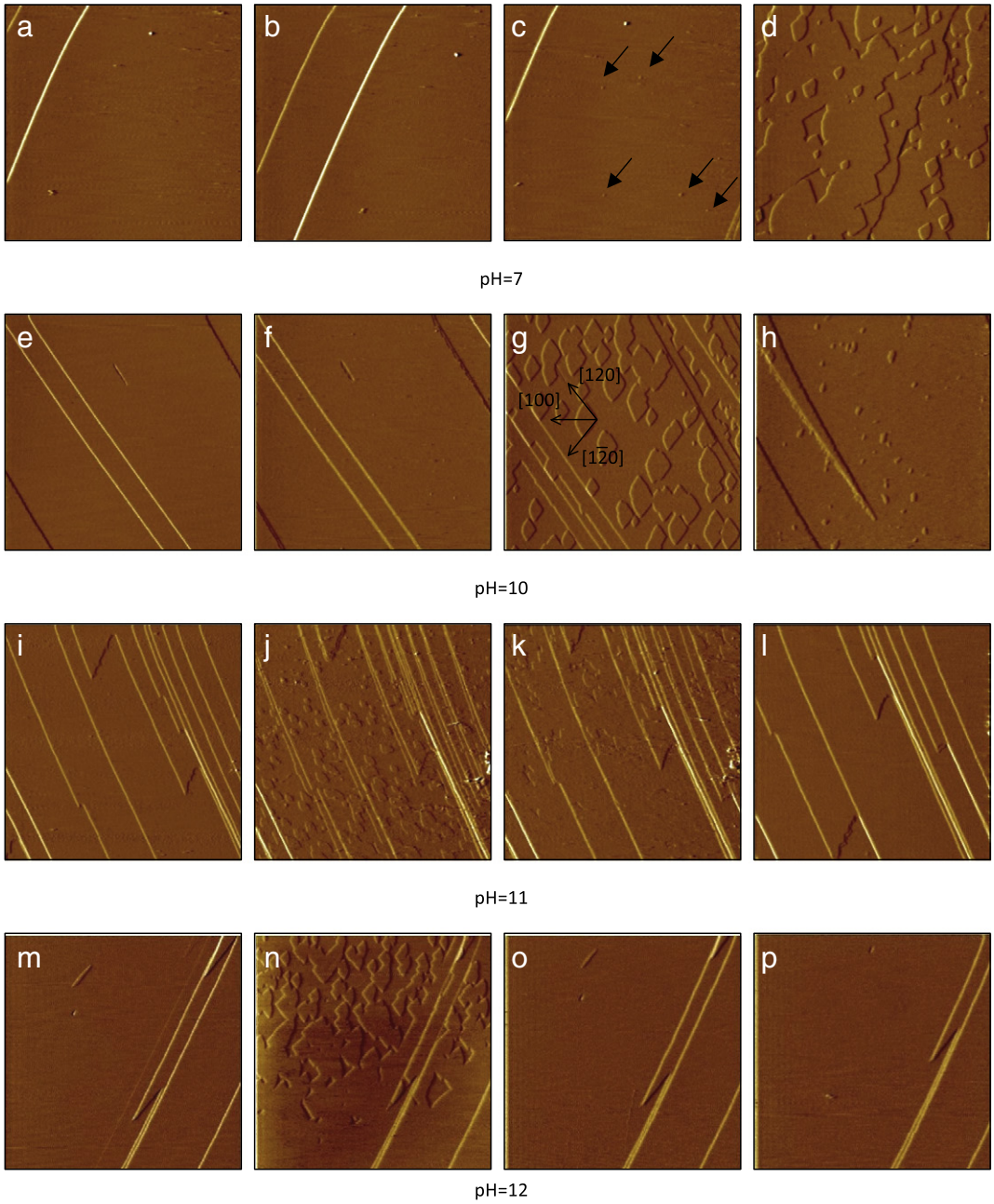

Fig. 1. AFM deflection images. Evolution of barite growth in different pH solutions. a–d: neutral pH. a) Barite substrate (001) before injecting pH growth solution, b) 100 s after injection, c) 200 s after injection, d) 2000 s after injection. Two different layers with different orientations of islands can be observed. In c) arrows point to the first appearance of nuclei. e–h: pH 10. e) Barite substrate before injecting growth solution, f) 100 s after injection, g) 800 s after injection, h) 4600 s after injection. Once the first layer was completed in approximately 2000 s only a few nuclei were observed. i–l: pH 11. i) Barite substrate before injecting growth solution, j) 100 s after injection, k) 200 s after injection, l) 1500 s after injection. No more growth was observed after the first layer. m–p: pH 12. m) Barite substrate before injecting growth solution, n) 100 s after injection, o) 200 s after injection, p) 2000 s after injection. No more growth was observed after the first layer.

between enthalpies at different pH values of the precipitating solution. Similar experiments (Kowacz et al., 2010) were carried out to detect the changes in enthalpy of barium sulfate precipitation in the presence of different background electrolytes (KCl, NaCl, LiCl, NaBr or NaF).

3. Results

3.1. AFM observations of barite surface nucleation and growth rate

3.1.1. Growth rates along [100] crystallographic direction

The main growth mechanism at the saturation state used for all AFM experiments (SI = 0.92–0.94) was island nucleation and spreading, as seen in Fig. 1. The growth islands showed a characteristic circular sector shape with two straight sides and a curved side forming an obtuse angle (~105°) at the apex of the sector (Fig. 1g). The [100] direction is along the radial direction of the sector. Growth rates were measured along the [100] direction in order to compare the influence of pH on the kinetics of barite growth. While injecting the growth solution into the AFM fluid cell, 2D islands could be observed nucleating and growing. From post-experiment measurements, the height of the 2D islands was found to be ~3.5 Å, corresponding to half a unit cell of barite. Barite islands grew, merged and eventually formed a new layer on the cleaved surface. Before this new growth layer was completed, new islands nucleated on top of it with the opposite orientation due to the 2_1 screw symmetry axis parallel to [001] (Pina et al., 1998), see Fig. 1g. The measured growth rates are given in Table 2.

Growth rates between pH 3 and pH 9 did not vary significantly but at both low (pH 2) and high pH (10, 11 and 12) the rates were significantly faster. In neutral solutions, the growth rate along [100] was 0.37 ± 0.03 nm s^{-1} and the values for solutions pH 3 to pH 9 varied from 0.41 ± 0.07 nm s^{-1} to 0.39 ± 0.04 nm s^{-1}. However, when growth solutions of pH 2 and pH >9 were tested, an increase in growth rate was observed as can be seen in Fig. 2 and Table 2. The growth rate measured at pH 2 was 1.15 ± 0.12 nm s^{-1} significantly higher than rates in the range of pH 3–9. For pH 10, 11 and 12 growth rates increased sharply, reaching a value of 10.62 ± 1.02 nm s^{-1} at pH 12.

The additional growth experiments performed at neutral pH in which NaCl was added to obtain the same IS as that of the growth solutions of pH 2, pH 10 and pH 11 (Table 1) showed that growth rates are higher in highly alkaline solutions (pH 10 and pH 11) than the rates measured in solutions at neutral pH but with the same ionic strength. However, growth rates measured at pH 2 were similar to those determined at neutral pH and the same IS (Table 2).

As seen in PHREEQC calculations, solution speciation is also modified with changes in pH (Table 1). With increasing pH of the growth solution, the molar concentration of $BaCl_2$ and Na_2SO_4 in the solutions had to be slightly adjusted in order to keep the saturation state (SI_{Barite}) constant as the activity of $BaOH^-$ and $BaCO_3^0$ increases. Otherwise, no significant changes in the concentration of the different species were found at neutral–high pH. However, it is worth noting that at acidic pH the concentration of HSO_4^- increases sharply from pH 3 to pH 2, so that the concentration of $BaCl_2$ and Na_2SO_4 in the growth solution at pH 2 had to be almost doubled (compared with the concentration at neutral pH, Table 1) in order to maintain the same concentration of Ba^{2+} and SO_4^{-2} ions (the ratio of activities was $a[Ba^{2+}]/a[SO_4^{-2}] = 1.64$).

Table 2
Growth rates measured for different pH values of growth solutions along the [100] crystallographic direction (nm/s) and the calculated errors. The last three rows correspond to experiments made to test the IS (ionic strength) effect on the growth rate. They were made without varying the natural pH of the growth solutions (5.5–6).

pH	Growth rates along [100] (nm/s)
2	1.15 ± 0.12
3	0.36 ± 0.07
4	0.31 ± 0.01
5	0.28 ± 0.02
7	0.37 ± 0.03
9	0.39 ± 0.04
10	0.54 ± 0.05
11	1.64 ± 0.30
12	10.62 ± 1.02
pH 7 (IS as pH 10)	0.43 ± 0.03
pH 7 (IS as pH 11)	0.60 ± 0.08
pH 7 (IS as pH 2)	0.99 ± 0.13

3.1.2. Surface nucleation density and induction time

Quantification of the nucleation density for each solution tested in AFM experiments was made from counting the number of nuclei in a given area. At neutral pH, black arrows on Fig. 1c indicate the first nuclei that appeared. For alkaline solutions, a clear increase in nucleation density was observed with increasing pH values of the growth solutions, especially in the range pH 9–12. However, at low pH, the nucleation density was lower than for neutral and high pH solutions and in the particular case of pH 3 only few isolated islands were systematically observed in five replicated experiments (Fig. 3).

Similar difficulties to exactly determine representative values of induction time were found. Nevertheless, a general and clear trend observed was that nucleation from alkaline solutions was much faster and so the induction time was reduced with increasing pH. At neutral pH, the first nuclei were observed after 200 s of injecting growth solution. At pH 9 and pH 10 we observed 2D nucleation in less than 100 s after injecting growth solution and at pH 11 and pH 12 the nucleation event happened immediately on contact of the growth solution with the barite surface. At low pH (except at pH 2, see below) due to the slow nucleation and the low nucleation density, a value for induction time was difficult to determine precisely. Overall, the tendency observed after several replications were performed was an increase in the induction time for pH ≤7 to pH 3, where the longest induction time (ca. 500 s) and the lowest nucleation density (0.04 islands per μm^2) were measured. Note that the value measured at pH 12 was 8.75 islands per μm^2. For the particular case of pH 2, islands appeared on the surface immediately after injection of the growth solution and the nucleation density was significantly higher than for pH 3 but still far from the high values obtained in alkaline solutions (Fig. 3).

In terms of nucleation rates, for increased $IS_{pH\ 10}$, $IS_{pH\ 11}$ and $IS_{pH\ 2}$ solutions, the first islands did not appear immediately after injecting the solution at pH 11 and pH 2. Islands appeared around 150 s after injection of growth solution. Clearly the induction time was slower than in pH 10, pH 11 and pH 2. The nucleation density obtained with $IS_{pH\ 10}$, $IS_{pH\ 11}$ and $IS_{pH\ 2}$ solutions was lower than for pH 10, pH 11 and pH 2 (Table 2).

3.1.3. Self-inhibiting layer and precipitate formation at alkaline pH

In pH 11 and pH 12 growth solutions, fast nucleation and growth were first observed on the initial barite layer; however, once the first growth layer was completed, no further layers developed. When the pH 10 growth solution was injected into the fluid cell, fast growth was observed on the initial layer; subsequently, a few nuclei formed on top but they did not develop as characteristic sector-shaped islands and even after 4600 s of continuous injection of growth solution they remained as small irregular nuclei (Fig. 1h).

AFM recovery experiments with growth solutions of the same pH but higher SI (1.36) were performed once the "self-inhibiting" layer was developed at pH 11 on the barite (001) surface. These recovery solutions were injected continuously for approximately 20 AFM scans (ca. 1800 s). Growth was resumed under these conditions but the $BaSO_4$ islands were distorted from the normal sector shape presenting rounded and irregular lens shapes. Again, after the first layer was completed, growth stopped. To recover growth again a higher SI (SI = 1.5) solution was used. Interestingly, at high pH values (10, 11 and 12) a precipitate was also observed forming on the barite surface. This precipitate

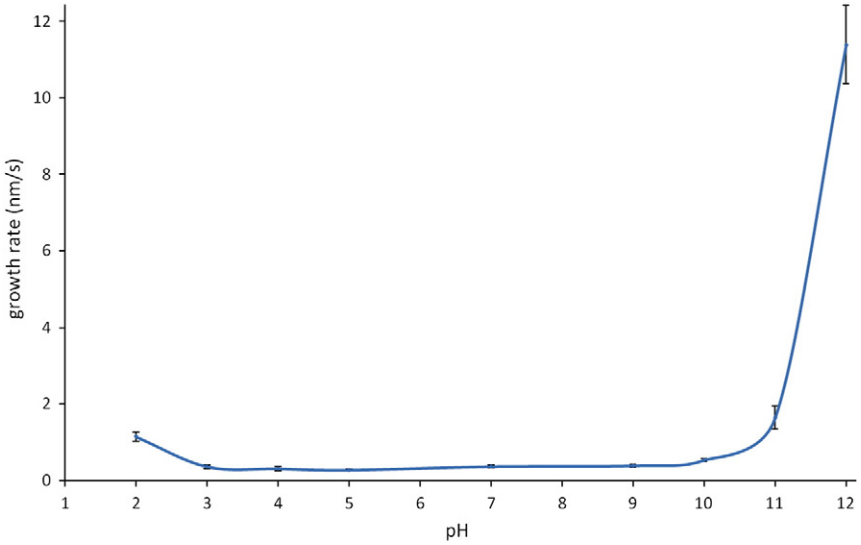

Fig. 2. Dependence of island growth rates (nm/s) in the [100] crystallographic direction on the pH of the growth solution.

had a gel-like appearance and the AFM tip partly swept it away while scanning. An attempt was made to analyze the surface precipitates ex situ using Raman spectroscopy (Horiba Yvon XploRA) but no other phase apart from barite was detected. A small thickness of a precipitated layer makes identification by Raman spectroscopy problematic because the axial resolution of the Raman system is typically in the order of a few micrometers. Hence, if the layer is considerably thinner than a micrometer, the Raman laser will mostly probe the underlying barite.

3.2. Nucleation experiments

3.2.1. Induction times and interfacial tension

A summary of the results of the spectrophotometer experiments (induction times and the values of interfacial tension calculated) is given in Table 3. These results are only used to compare the relative effects of pH on both variables and are not aimed at determining absolute values. As can be seen in Table 3, the interfacial tension was reduced up to pH 10. With pH 11 and 12 the values fluctuated slightly but are still lower than values for neutral solutions. These values were significantly lower than values obtained for $BaSO_4$ published by other authors (e.g. Söhnel, 1982; Fernández-Díaz et al., 1990). Thus, although they may not allow us to obtain absolute values to compare with other published studies, they can still be used to compare the relative differences in interfacial tension values between different pH solutions employed in this study under our experimental conditions.

3.2.2. Conductivity experiments

These experiments give another estimation of the precipitation rate of $BaSO_4$ when different pH solutions were tested. In Fig. 4 representative curves of the evolution of conductivity are plotted against time for different pH values. As shown in Fig. 4, the induction time was close to 0 in all the pH tested. As shown in Fig. 5, the slope of the linear regime of the conductivity curve increases with increasing pH of the growth solutions. These results are in agreement with the observations previously made in the turbidity experiments, and indicate faster precipitation rate with increasing pH.

3.2.3. Morphology of barite particles

FESEM observations of particles obtained in turbidimetry experiments at $1.5 \cdot 10^{-4}$ M $BaSO_4$ concentration indicate that the morphology

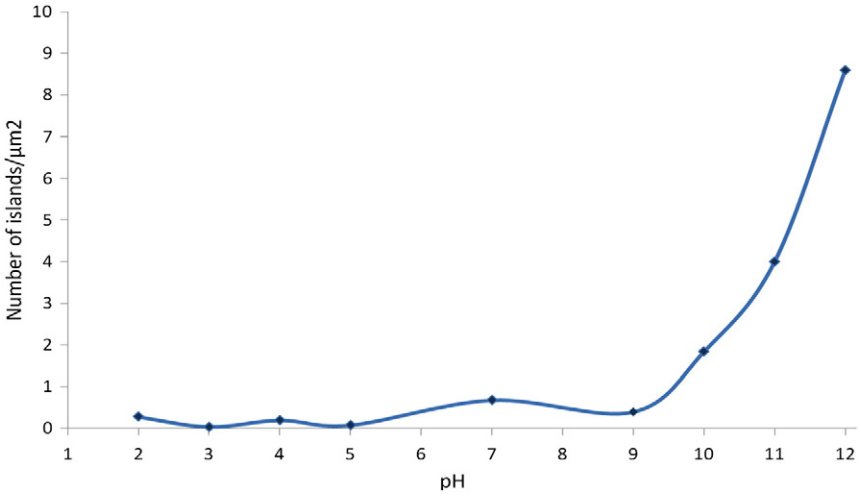

Fig. 3. Number of growth islands formed as a function of pH on a barite (001) surface after 250 s of growth solution injection. The trend for pH 9 to pH 3 showed similar results within experimental error. For pH 10 and higher pH the nucleation density was greatly enhanced. Below pH 3 the number of islands also slightly increases.

Table 3
Summary of the results obtained from the spectrophotometer experiments and the results of the interfacial tension obtained. As can be seen, the values of interfacial tension calculated were lower in high pH solutions and in pH 2 than the value obtained for neutral solutions.

Experiment number	Supersaturation β_{Barite}	pH	Induction time (s)	γ (mJ/m2)
A1_0	288	7	289	22.8 ± 0.42
A1_1	427	7	246	
A1_2	589	7	95	
A1_3	759	7	46	
A1_4	955	7	28	
A1_5	1380	7	17	
B_0	295	8,5	263	21.31 ± 0.39
B_1	589	8,5	79	
B_2	955	8,5	37	
B_3	1380	8,5	21	
C_0	174	10	190	18.3 ± 1.48
C_1	288	10	78	
C_2	427	10	31	
C_3	589	10	32	
C_4	759	10	26	
C_5	955	10	17	
D_0	162	11	322	19.32 ± 1.09
D_1	269	11	209	
D_2	407	11	96	
D_3	562	11	77	
D_4	724	11	48	
D_5	912	11	21	
D_6	1318	11	11	
E_0	107	12	338	17.89 ± 1.08
E_1	282	12	138	
E_2	398	12	44	
E_3	661	12	26	
E_4	1000	12	14	
D_0	110	2	561	17.78 ± 0.44
D_1	170	2	192	
D_2	240	2	97	
D_3	407	2	68	
D_4	617	2	37	

of $BaSO_4$ particles evolves towards more equidimensional shapes and smaller sizes with increasing pH. The average particle size in the neutral solution for this concentration was measured and found to be 14 × 7 μm. The size decreased to 5 × 5 μm at pH 11 at the same molar concentration. The thickness of the barite particles increases also with increasing pH (Fig. 6) from 10–50 nm to 500 nm at pH 11.

Even though the SI is slightly lower when pH is increased, faster nucleation and a reduction in induction times can be inferred from the increase in the number of particles (Mullin, 1992). Although it is difficult to precisely quantify the density of precipitated particles, a rough estimation based on FESEM observations of representative areas of the filter membranes indicates that the number of particles obtained increased with increasing pH up to pH 11 and then decreased very significantly at pH 12 (for $1.5 \cdot 10^{-4}$ M $BaSO_4$). At pH 12 and $1.5 \cdot 10^{-4}$ M $BaSO_4$, the shape of the barite particles obtained was significantly distorted (Fig. 6e) from the normal square–rectangular shape, and very few barite particles were observed. It is also noted that at pH 12 branch-shaped particles were also observed (Fig. 6f and g). The EDX analyses of these particles showed peaks for barium, carbon and oxygen, while no sulfur was detected (Fig. 7). These particles were exclusively found at pH 12, and as discussed below, they are most likely barium carbonate.

3.3. Effect of pH on Ba^{2+} hydration

The enthalpy of precipitation of $BaSO_4$ is given by:

$$\Delta H_{ppt} = U(BaSO_4) + \Delta H_{dehyd}(\text{ions})$$
$$\Delta H_{ppt} = U(BaSO_4) - \Delta Hhyd\left(Ba^{2+}\right) - \Delta Hhyd\left(SO_4{}^{-2}\right)$$

where U ($BaSO_4$) is the lattice energy; ΔH_{hyd} (Ba^{2+}) is the enthalpy of hydration of Ba^{2+}; ΔH_{hyd} (SO_4^{-2}) is the enthalpy of hydration of $SO4^{-2}$.

Lattice energy does not depend on the solution composition and so by comparing the changes in ΔH_{ppt} values we can obtain an estimate of the effect of the pH variation on the hydration enthalpy of the Ba^{2+} and SO_4^{-2} ions.

The results of our calorimeter experiments showed small changes in enthalpy of precipitation of $BaSO_4$ when the pH of the solution varies (Table 4), but they were within the error of the measurements and therefore no definite conclusion could be reached. Kowacz et al. (2010) interpreted observed changes in enthalpy to be related to changes in the hydration of Ba^{2+} and SO_4^{-2} ions but in our experiments, no changes were detected from the calorimetry measurements.

4. Discussion

4.1. Limiting processes for surface nucleation and growth

The results of this study show that the pH of the solution from which barium sulfate nucleates and grows influences the kinetics and mechanism of such processes, particularly at high pH. Direct AFM observations show that growth rates measured along the [100] crystallographic direction on barite (001) cleavage surfaces increase rapidly above pH 9 of the growth solutions (see Fig. 2 and Table 2). The nucleation event is a strongly surface-dependent process and, although not easy to quantify, we observed a large increase in 2D-nucleation rate and density of sector shape islands on barite surfaces from high pH growth solutions (Figs. 1 and 2).

2D surface nucleation and growth are more likely limited by the probability of contact of a barium ion in a "dehydrated state" with the crystal surface (Piana et al., 2006) and this is controlled by the frequency of water exchange that determines dehydration rates and mobility of ions in solution (Kowacz et al., 2010). The molecular dynamic simulations performed by Piana et al. (2006) showed that although sulfate anions can easily aid in the desolvation of the crystal surface, nucleation is only induced by barium adsorption that is assisted by the surface deposition of sulfate anions. From these results, it is hypothesized that any factor modifying solute or surface hydration (e.g. specific characteristics of the background electrolytes present) can affect 2D-nucleation and ion incorporation at kink sites (e.g. Kowacz and Putnis, 2008). The fact that the structure of the solvent strongly influences crystallization processes is well documented. Hribar et al. (2002) stated that ions in solution affect the structure of water and this is the result of the balance between electrostatic forces (the water molecule dipole) and hydrogen bonding (water–water interactions). Ion hydration results from the competition between hydrogen bonds between water molecules and electrostatic forces established between the water dipoles and any other ions present in solution.

4.2. Effect of hydroxyl ions on solvent structure and the hydration of building units

As the growth of barite from solutions of the same SI but pH 3–10 is similar and only differs at low and high pH, we explore the possibility that the effect of H^+ and OH^- ions on the solvent structure, the hydration of barite surfaces and the hydration–dehydration of barite building units (Ba^{2+} and SO_4^{2-}) may be responsible for the observed changes on barite nucleation and growth especially at high pH.

Ab initio simulations carried out by Tuckerman et al. (1995) showed that OH^- and H^+ ions have different behaviors. In acidic solutions, the excess proton H^+ is associated with the oxygen atom of a water molecule forming the hydronium ion (H_3O^+) and its associated complexes, which integrate naturally into the hydrogen bond network without introducing a significant rearrangement of the solvent. H^+ does not have as strong effect on the interaction between water molecules as OH^- does, the latter introducing a strong local order. Furthermore, the

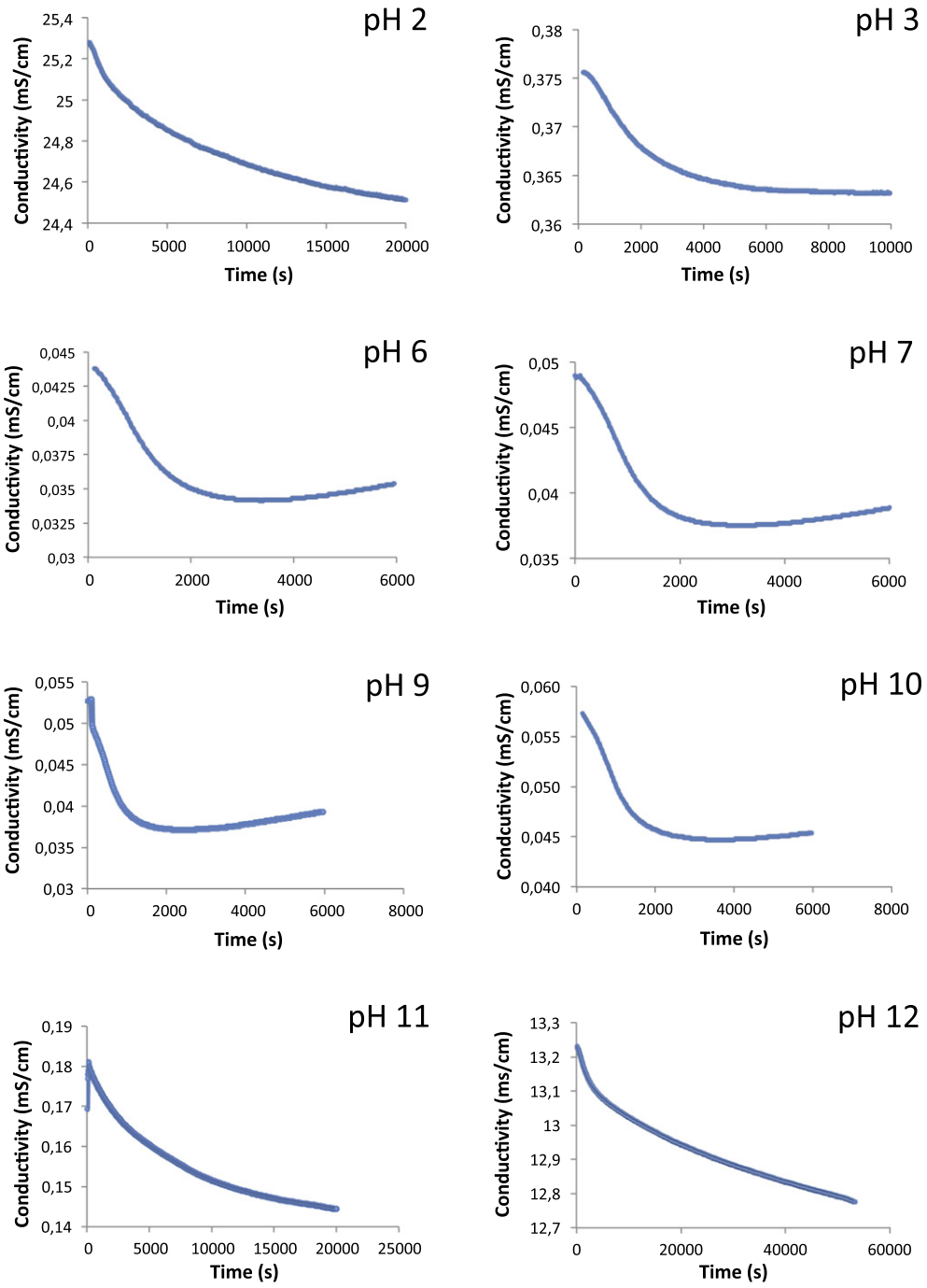

Fig. 4. Representative curves obtained from conductivity experiments. Specific conductance (mS/cm was monitored against time. The slope of the conductivity curve in the linear regime is related to the precipitation rate.

effect of H^+ on barite nucleation and growth is not expected to be as important, because solvent structure in the vicinity of Ba^{2+} will be determined by oppositely charged ions (Kowacz and Putnis, 2008) and experimental evidence from Kowacz et al. (2007) supports the hypothesis that desolvation of Ba^{2+} is the rate limiting process for $BaSO_4$ crystal growth.

OH^- is known as being a structure-maker ion or kosmotrope ion and tends to form a clearly identifiable hydration shell in which water molecules are strongly reoriented and bonded and this yields to a strong perturbation in the hydrogen bond network. This stable hydration shell is due to the high charge density of hydroxyl ions (Tuckerman et al., 1995). In alkaline solutions, the high concentration of hydroxyl ions (OH^-) is expected to introduce a significant reorganization of the solvent structure and consequently change the hydration of ion building units in solution that would be finally reflected in changes in growth and nucleation rates.

4.3. Effect of pH on 2D surface nucleation and growth (AFM observations)

The previous discussion provides a framework for the rationale of the observed effect of pH on 2D surface nucleation and growth of barite. When increasing the pH of the growth solutions above pH 10, nucleation rates as well as the density of islands on the surface were significantly enhanced. This effect may be related to the increasing

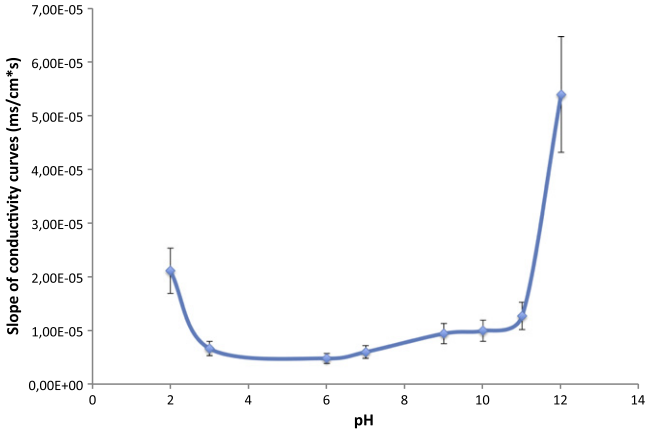

Fig. 5. Slope of the conductivity curves plotted against pH. As can be seen, the slope of the conductivity curve increases with increasing pH, which is related to faster precipitation rates.

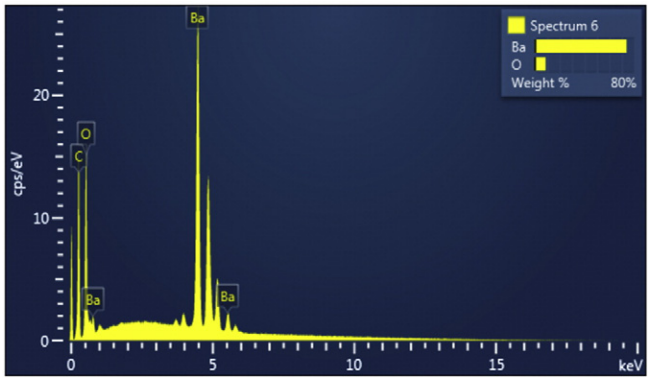

Fig. 7. Energy dispersive X-ray analysis of particles obtained from turbidity experiments at pH 12 (Fig. 6g). Peaks for barium, carbon and oxygen can be seen while no sulfur was detected. These particles were exclusively found at pH 12, and as discussed, they are possibly barium carbonate.

concentration of OH^- ions in growth solutions of pH 10, 11 and 12. The effect of hydroxyl ions can be understood in the same way as the presence of other background ions in solution (e.g. Kowacz and Putnis, 2008; Ruiz-Agudo et al., 2011). Its structure-making character increases the competition for water molecules between building units, OH^- and water itself, which implies an increase (compared with neutral and low pH solutions) in the mobility of water molecules in an ion's hydration shell and in water molecules on the mineral surface. When hydroxyl ions are present, water is less mobile around them and thus, relatively more mobile around Ba^{2+} and SO_4^{-2}. An increase in mobility of water molecules in the hydration shell of barite building units in the presence of OH^- (i.e. shorter residence time of H_2O molecules in Ba^{2+} and SO_4^{-2} hydration shells), would increase the probability that a desolvated

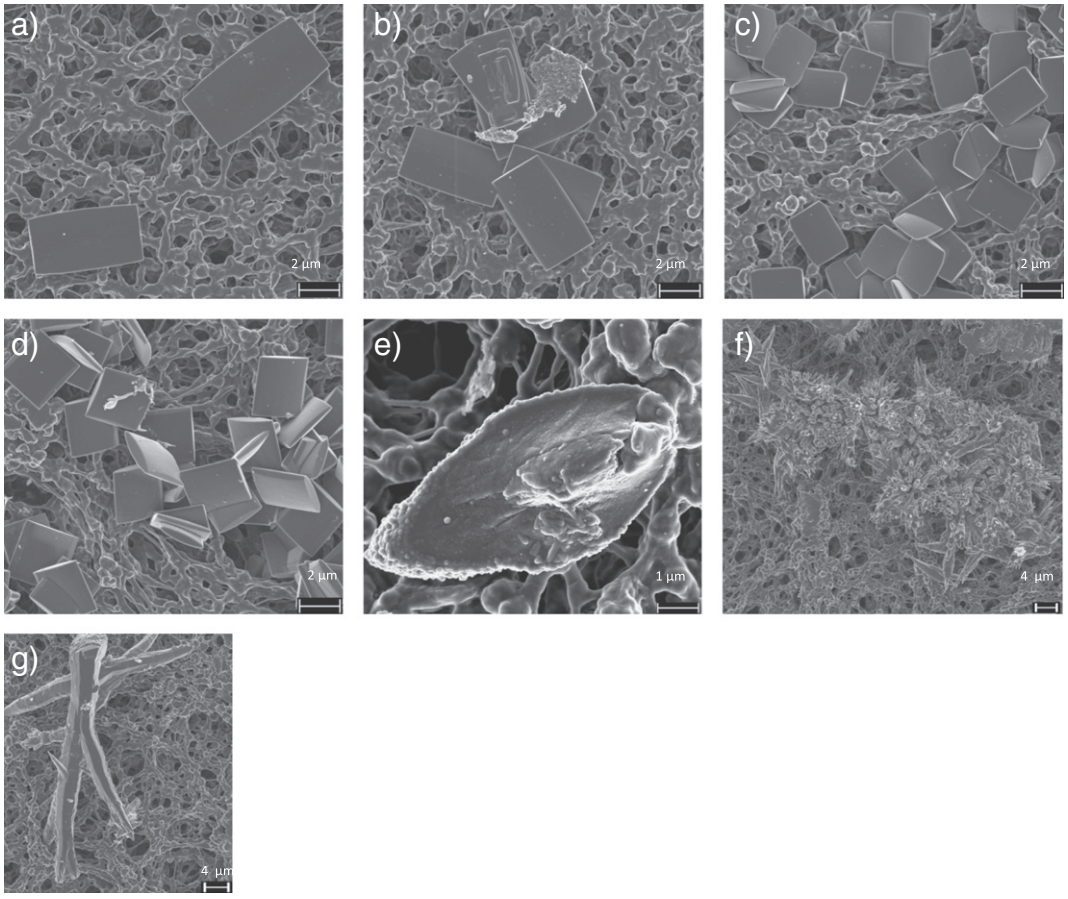

Fig. 6. FESEM observations of barium sulfate particles obtained from nucleation experiments. a) pH 7 growth solution and SI (saturation index) 2.32. b) pH 8.5 and SI 2.32. c) pH 9.5 and SI 2.32. d) pH 11 and SI 2. 28. e) pH 12 and SI 2.09. Only a few particles were found at pH 12, possibly due to the lower SI of the growth solution. The shape of the precipitate was distorted from the normal rectangular-pillow shape. f) and g) In pH 12 solution new particles were observed. They are possibly $BaCO_3$ after morphological comparison with witherite particles obtained by Chen et al. (2001).

Table 4
Barium concentrations after mixing the solutions in the calorimeter and related data: SI - supersaturation with respect to $BaSO_4$; concentration of $[Ba^{2+}]$ measured in solution after the precipitation reaction (final concentration) expressed in μM and as the percentage of barium in solution with respect to the initial value (relative $[Ba^{2+}]$ = % of initial $[Ba^{2+}]$); $QBaSO_4$ — heat of $BaSO_4$ precipitation; ΔH_{ppt} — enthalpy of precipitation.

pH	Initial concentration	SI	Final concentration			$QBaSO_4$		ΔH_{ppt} (kJ/mol)
	$[Ba^{2+}]$ μM		$[Ba^{2+}]$ (μM)	S.D. ± (μM)	Relative $[Ba^{2+}]$ = % of ini. $[Ba^{2+}]$	(J)	S.D. ± (J)	
2.0	248.83	2.24	1.12	±0.22	0.45%	4.69	±0.42	−9.97
7.0	248.27	2.70	0.92	±0.58	0.37%	4.40	±0.38	−6.79
8.4	246.32	2.70	1.10	±0.27	0.45%	5.16	±0.26	−7.95
9.8	246.92	2.69	0.82	±0.29	0.33%	5.03	±0.67	−7.75
10.5	247.57	2.68	1.14	±0.17	0.46%	4.99	±0.28	−7.67
11.3	248.04	2.63	0.69	±0.15	0.28%	4.39	±0.10	−6.74

barium ion can attach to the $BaSO_4$ surface and create a 2D-nucleus. This would explain the increase in growth rates and in 2D nucleation at high pH.

At neutral and mildly acidic pH (pH 3–7), growth rates did not vary significantly. This would be easily understood considering that H_3O^+ ions integrate into the water structure without causing significant distortion of solvent structure (Tuckerman et al., 1995). As already stated, pH 2 growth solutions resulted in enhanced induction times and nucleation density compared to growth at pH 3. Under the former conditions, the ratio of barium and sulfate activities was different from 1 ($a[Ba^{2+}] / a[SO_4^{-2}] = 1.64$). Kowacz et al. (2007) showed that barite growth and nucleation depend strongly on the barium to sulfate activity ratio. Thus, it is likely that the higher activity of barium with respect to sulfate at pH 2 results in the observed enhancement in the nucleation density and appearance of islands immediately after injection, and it cannot be confidently attributed to an effect of pH. This promotion of nucleation when $Ba^{2+} > SO_4^{2-}$ was used by Kowacz et al. (2007) to corroborate the hypothesis that the rate limiting step for 2D nucleation is the barium incorporation which is also enhanced in the presence of higher concentrations of Ba^{2+}.

4.4. Effect of pH on 3D nucleation (bulk experiments)

The interfacial surface tension (γ) between a solid and the solution controls the kinetics of nucleation (Söhnel, 1982). Any factor reducing the solid–liquid interfacial tension should reduce the nucleation barrier. The interfacial tension measured from bulk precipitation experiments was reduced when the pH of the solution increased (Table 3). The values obtained are significantly lower than data reported by other authors. This suggests that nucleation may take place in the heterogeneous regime in our experiments. In any case, shorter induction times with increasing pH indicate enhanced nucleation at alkaline conditions. Furthermore, SEM observations show that at higher pH values, the $BaSO_4$ particles display smaller sizes, in good agreement with the shorter induction times determined under such conditions (Fig. 6). The nucleation rate determines the size of the particles obtained in precipitation experiments. High density of particles and small particle size is related to high nucleation rates while low density of particles and larger sizes are attributed to lower nucleation rates (Mullin, 1992). These results, together with those from conductivity experiments, where precipitation rates increase with increasing pH of the solutions, are consistent with the conclusions derived from AFM experiments and suggest that an increase in pH accelerates barite nucleation. Again, increased frequency of water exchange in the solvation shell of barite building units (especially in the hydration of Ba^{2+}) due to the presence of high concentrations of OH^- ions could explain the enhancement in barite nucleation inferred from the different experiments.

Furthermore, the SEM observations suggest that with increasing pH the morphology of barite crystals evolves towards a more equidimensional form. This effect is interpreted to be related to the chemisorption of hydroxyl or carbonate ions onto specific faces (Sánchez-Pastor et al., 2013). According to previous work, barite crystals with equidimensional morphologies may result from the overdevelopment of the (001) face (Jones and Ogden, 2010; Massi et al., 2010). This could be the result of retarded growth rate of this face relative to other barite faces due to the chemisorption of foreign ions, possibly hydroxyl or carbonate ions (Sánchez-Pastor et al., 2013) that would make this face more important in the final habit of the crystal.

4.5. Self- inhibiting layer and surface precipitates

Our observations at high pH differ from barite growth observations at neutral pH reported in previous work (e.g. Pina et al., 1998; Risthaus et al., 2001; Kowacz and Putnis, 2008). In the AFM growth experiments performed at high pH (10–12), we observed the formation of a self-inhibiting first layer that grew rapidly, resulting in the reproduction of the original surface topography, but was followed by reduced nucleation and growth on subsequent layers. A similar phenomenon has been reported by Astilleros et al. (2002) and Higgins and Hu (2005) who demonstrated that the growth rate of each monolayer depends on the crystallographic characteristics of the previous layer (i.e. the "template" effect). This was interpreted to be related to changes in the structure or composition of newly grown layers due to incorporation of 'foreign' ions with the consequent changes in unit cell dimensions. Our experimental results at high pH showed that the recovery of growth on a self-inhibiting layer needed a higher SI of the growth solution. Nuclei generated on top of the first layer after injecting this higher SI solution do not display the normal island growth sector shape, but rather a distorted morphology. The measured height of the newly-grown first layer is ~3.5 Å, that is not significantly different from that of pure barite (within the experimental error). Chemical characterization of such a thin layer by ex-situ Raman analysis failed to give any conclusive result.

However, given that this self-inhibiting layer forms only at high pH, it seems reasonable to assume that it is associated with the presence of either OH^- or CO_3^{2-} ions during growth under highly alkaline conditions. Note that alkaline solutions are prone to absorb significant amounts of CO_2 and once dissolved and hydrolyzed, carbonate species in solution may well incorporate into growing barite. Incorporation of foreign ions into growing crystals is known to alter the structure of the substrate on which barite is growing, causing the inhibition of the second and successive layers. The observed distorted shape of the islands, when a solution with a higher supersaturation with respect to barite was injected with the aim of recovering growth on top of the inhibiting layer, could be an indication of the alteration in the structure of the newly grown layer. Understanding the mechanism by which the first grown monolayer controls the growth behavior of the next layers is hypothetical, although a likely explanation for such an observation has been provided by Astilleros et al. (2010). These authors suggest that relaxation of the strain associated with the formation of a thin layer of a solid solution growing epitaxially on a substrate introduces variations in bond lengths and departure from the ideal crystal topography. According to these authors, the distribution of the "foreign" ions will be predetermined by the structure of the underlying layer and the interactions between the ions, resulting in a decrease in the activation

entropy for the growth of this layer and, as a consequence, in a decrease in the growth rate or even the complete arrest of growth. This may as well explain observations by Sánchez-Pastor et al. (2013), who found that carbonate ions have different effects on successive layers formed on barite during growth. In this work, the spreading rate of the first layer grown on a pristine barite surface increases slightly with carbonate content, while the growth of the second layer is notably inhibited at a carbonate activity of $6.6 \cdot 10^{-5}$ M. This effect is ascribed to carbonate incorporation into barite (shown by Raman spectroscopic analysis). Note however that the pH (and the OH^- concentration) increases as well with carbonate concentration in their experiments. Moreover, in our experiments complete blockage is achieved at significantly lower carbonate activity ($1.2 \cdot 10^{-5}$ and $1.1 \cdot 10^{-5}$ at pH 11 and 12, respectively). This suggests that OH^- trapping or incorporation (and not exclusively carbonate ions) may also contribute to the observed "poisoning" of the barite surface in our system. Similar effects (i.e. "normal" growth of the first layer and different growth behavior for second and successive layers) have been previously reported for other minerals such as calcite (i.e. Pérez-Garrido et al., 2007, 2009; Astilleros et al., 2010).

Together with the inhibition of growth, at pH values of 10, 11 and 12 of the growth solution, another type of precipitate was observed to form on the barite surface. It had a gel-like appearance, and was easily removed by the AFM tip indicating no significant crystallographic matching. Furthermore, ex-situ FESEM-EDX chemical analysis of particles obtained in bulk experiments (Fig. 6g) and assumed to be equivalent to the gel-like precipitate observed in AFM experiments, showed peaks only for barium, oxygen and carbon (Fig. 7). Based on PHREEQC thermodynamic calculations, no other phases apart from barium sulfate are expected to form in the system. The SI with respect to $Ba(OH)_2 \cdot 8H_2O$ calculated by PHREEQC is −9.10, −7.12 and −5.23 for pH 10, 11 and 12 growth solutions, respectively. The bulk solution is also undersaturated with respect to barium carbonate ($BaCO_3$) according to PHREEQC thermodynamic calculations (SI of −1.29, −0.89, and −0.95 for pH 10, 11 and 12, respectively). Thus the bulk solutions are far from equilibrium with respect to both phases. Nevertheless, the formation of these phases cannot be ignored as, frequently, dissolution–precipitation reactions occurring at the mineral–fluid interface are determined by the composition of the fluid at the mineral surface, that can differ significantly from the composition of the bulk solution (Ruiz-Agudo et al., 2014). By comparison with published morphologies for $BaCO_3$ (Chen et al., 2001), it seems likely that the branch-shaped particles obtained in our batch experiments at pH 12 and $1.5 \cdot 10^{-4}$ M of $BaSO_4$ (and by inference, the gel like precipitate formed in AFM experiments) are $BaCO_3$.

5. Conclusions

Both AFM and bulk experiments show that barite nucleation and growth are not significantly affected by pH in the range 3–9 but are significantly promoted at alkaline pH (10–12). The higher concentration of kosmotrope (structure-maker) OH^- ions present at high pH could increase the frequency of water exchange between Ba^{2+} hydration shells and the bulk water as well as help the desolvation of barite surfaces. This would eventually facilitate barite 2D-nucleation and growth, as suggested by the increase in the density of growth islands and the sharp increase in growth rates observed in AFM experiments. However, at high pH this growth is restricted to the initial growth layer after which the surface becomes passivated. This may be related to a surface distortion caused by trapping of foreign ions (hydroxyl or carbonate) during barite growth under highly alkaline conditions. Chemisorption of these foreign ions and subsequent retardation of the growth of the (001) face may be responsible for the observed change in morphology at high pH.

Furthermore, the reduction in interfacial tension (determined from bulk measurements of induction times at different supersaturations) and the increase in nucleation rate at high pH (deduced from the smaller particle sizes and higher density of particles found in bulk precipitation experiments at high pH) are in good agreement with the surface processes observed directly by AFM. These results give us a baseline for discerning the barite growth modifications introduced by the addition of additives, such as inhibitors that are generally more effective at pH >7. Furthermore, this study provides insights into the mechanisms by which electrolytes may modify solvent structure and ion hydration and ultimately influence mineral growth.

Acknowledgments

This research was carried out within a Marie Curie initial training network from the European Commission (MINSC ITN 290040). The authors thank Manuel Prieto Rubio for the use of the calorimetry equipment at Oviedo University and as well for valuable discussions. E R-A also acknowledges the receipt of a Ramón y Cajal grant from the Spanish Government (Ministerio de Economia y Competitividad) as well as funding by the Spanish Government and European Commission (grant MAT2012-37584-ERDF) and the Junta de Andalucía (research group RNM-179 and project P11-RNM-7550).

We are thankful to the two anonymous reviewers for all the constructive comments that have helped us to improve the overall quality of our paper.

References

Astilleros, J.M., Pina, C.M., Fernández-Díaz, L., Putnis, A., 2002. Molecular-scale surface processes during the growth of calcite in the presence of manganese. Geochim. Cosmochim. Acta 66, 3177–3189.
Astilleros, J.M., Fernández-Díaz, L., Putnis, A., 2010. The role of magnesium in the growth of calcite: an AFM study. Chem. Geol. 271, 52–58.
Baynton, A., Ogden, M.I., Raston, C.L., Jones, F., 2012. Barium sulfate crystallization dependence on upper rim calix[4]arene functional groups. CrystEngComm 14, 1057–1062.
Blount, C.W., 1977. Barite solubilities and thermodynamic quantities up to 300 °C and 1400 bars. Am. Mineral. 62, 942–957.
Ceccarello, S., Black, S., Read, D., Hodson, M.E., 2003. Industrial radioactive barite scale: suppression of radium uptake by introduction of competing ions. Miner. Eng. 17, 323–330.
Chen, P.-C., Cheng, G.Y., Kou, M.H., Shia, P.Y., Chung, P.O., 2001. Nucleation and morphology of barium carbonate crystals in a semi-batch crystallizer. J. Cryst. Growth 226, 458–472.
Dove, P.M., Czank, C.A., 1995. Crystal chemical controls on the dissolution kinetics of the isostructural sulfates: celestite, anglesite, and barite. Geochim. Cosmochim. Acta 59, 1907–1915.
Fernández-Díaz, L., Putnis, A., Cumberbatch, T.J., 1990. Barite nucleation kinetics and the effect of additives. Eur. J. Mineral. 2, 495–501.
Hanor, J., 2000. Barite–celestite geochemistry and environments of formation. Rev. Mineral. Geochem. 40, 193–275.
Higgins, S.R., Hu, X., 2005. Self-limiting growth on dolomite: experimental observations with in situ atomic force microscopy. Geochim. Cosmochim. Acta 69, 2085–2094.
Hribar, B., Southall, N.T., Vlachy, V., Dill, K.A., 2002. How ions affect the structure of water. J. Am. Chem. Soc. 124 (41), 12302–12311.
Jones, F., Ogden, M.I., 2010. Controlling crystal growth with modifiers. CrystEngComm 12, 1016–1023.
Jones, F., Oliveira, A., Rohl, A.L., Parkinson, G.M., Ogden, M.I., Reyhani, M.M., 2002. Investigation into the effect of phosphonate inhibitors on barium sulfate precipitation. J. Cryst. Growth 237–239, 424–429.
Kowacz, M., Putnis, A., 2008. The effect of specific background electrolytes on water structure and solute hydration: consequences for crystal dissolution and growth. Geochim. Cosmochim. Acta 72, 4476–4487.
Kowacz, M., Putnis, C.V., Putnis, A., 2007. The effect of cation:anion ratio in solution on the mechanism of barite growth at constant supersaturation: role of the desolvation process on the growth kinetics. Geochim. Cosmochim. Acta 71, 5168–5179.
Kowacz, M., Prieto, M., Putnis, A., 2010. Kinetics of crystal nucleation in ionic solutions: electrostatics and hydration forces. Geochim. Cosmochim. Acta 74, 469–481.
Massi, M., Ogden, M.I., Radomirovic, T., Jones, F., 2010. Tetrazoles: a new class of compound for crystallization modification. CrystEngComm 12, 4205–4207.
Mullin, J.W., 1992. Crystallization. Butterwoth-Heinemann, Oxford.
Nielsen, A.E., Söhnel, O., 1971. Interfacial tensions electrolyte crystal-aqueous solution, from nucleation data. J. Cryst. Growth 11, 233–242.
Parkhurst, D.L., Appelo, C.A.J., 1999. Users guide to PHREEQC (version 2)—a computer program for speciation, batch reaction, one-dimensional transport, and inverse geochemical calculations. U.S. Geological Survey Water-resources Investigation Report (99–4259).
Pérez-Garrido, C., Fernández-Díaz, L., Pina, C.M., Prieto, M., 2007. In situ AFM observations of the interaction between calcite (10 1 4) and Cd-bearing aqueous solutions. Surf. Sci. 601, 5499–5509.

Pérez-Garrido, C., Astilleros, J.M., Fernández-Díaz, L., Prieto, M., 2009. In situ AFM study of the interaction between calcite {l014} surface and supersaturated MnH-CO-aqueous solutions. J. Cryst. Growth 311, 4730–4739.
Piana, S., Jones, F., Gale, J.D., 2006. Assisted desolvation as a key kinetic step for crystal growth. J. Am. Chem. Soc. 128, 13568–13574.
Pina, C.M., Becker, U., Risthaus, P., Bosbach, D., Putnis, A., 1998. Molecular-scale mechanisms of crystal growth in barite. Nature 395, 483–486.
Risthaus, P., Bosbach, D., Becker, U., Putnis, A., 2001. Barite scale formation and dissolution at high ionic strength studied with atomic force microscopy. Colloids Surf. A Physicochem. Eng. Asp. 191, 201–214.
Ruiz-Agudo, E., Putnis, C.V., Rodríguez-Navarro, C., Putnis, A., 2011. Effect of pH on calcite growth at constant aCa^{2+}/aCO_3^{-2} ratio and supersaturation. Geochim. Cosmochim. Acta 75, 284–296.
Ruiz-Agudo, E., Putnis, C.V., Putnis, A., 2014. Coupled dissolution and precipitation processes at mineral–fluid interfaces. Chem. Geol. 383, 132–146.
Sánchez-Pastor, N., Kaliwoda, M., Veintemillas-Verdaguer, S., Jordan, G., 2013. On the effect of carbonate on barite growth at elevated temperatures. Am. Mineral. 98, 1235–1240.
Söhnel, O., 1982. Electrolyte crystal—aqueous solution interfacial tensions from crystallization data. J. Cryst. Growth 57, 101–108.
Söhnel, O., Mullin, J.W., 1978. A method for determination of precipitation of induction periods. J. Cryst. Growth 44, 377–382.
Todd, A.C., Yuan, M., 1990. Barium and strontium sulfate solid solution formation in relation to North Sea scaling problems. SPE Prod. Eng. 5, 279–285.
Tuckerman, M., Laasonen, K., Sprik, M., 1995. Ab initio molecular dynamics simulations of the solvation and transport of hydronium and hydroxyl ions in water. J. Chem. Phys. 103, 150–161.
Van Rosmalen, G.M., 1983. Scale prevention with special reference to threshold treatment. Chem. Eng. Commun. 20, 209–233.